# A Superconducting Gravity Gradiometer Tool for Exploration

*J. M. Lumley*[1], J. P. White[1], G. Barnes[1], D Huang[1], H. J. Paik[2]*
[1]*ARKeX Ltd.*, [2] *University of Maryland*

**Summary**

Superconducting gravity gradiometry has long been recognised as a technique offering key advantages over competitive techniques with respect to obtaining gravity or gravity gradient data. Superconductivity and low temperatures confer low noise, negligible scale factor drift and mechanical stability. Additionally, a Superconducting Gravity Gradiometer (SGG) incorporates superconducting circuits which can be balanced such that its responses to gravity gradients are largely independent of all linear and angular accelerations applied to the instrument. This "balance" relies on the ability to set and maintain persistent currents in the various superconducting loops. What makes the SGG so attractive an instrument for both satellite and airborne operation is the complete absence of drift in these currents once they have been set. This means that the scale factors remain perfectly stable in time and can thus be balanced precisely, with excellent null stability.

The European Space Agency (ESA) recognised these advantages of the SGG and have continually supported the development of a satellite version of an SGG with Oxford Instruments. We shall report both numerical analysis and experimental results of our work on the ESA SGG. We shall also report on the design and analysis of the SGG we are proposing as an exploration tool. Our analysis indicates that it will be possible to build and operate an SGG in an airborne environment to achieve the accuracy required. This device will measure all linear and angular accelerations to which the SGG is subjected, as is the case for our spaceborne SGG. These outputs are used to correct the measured gravity gradient data. When used in conjunction with accurate GPS data, the acceleration outputs will be useful in their own right to directly measure the long-wavelength components of the gravity field over the region of interest.

## 1. Introduction

The principle that gravity gradiometry is potentially extremely useful for exploration has been established since the beginning of the 20th century when von Eotvos developed the first practical instrument. Although his torsion balance instrument was extremely sensitive, it was very slow, so the technique was largely abandoned even though it was successful in "finding" billions of barrels of oil. It is clear that an airborne gravity gradiometer with similar sensitivity to the original von Eotvos tool would be extremely powerful for exploration purposes.

This paper describes the superconducting gravity gradiometer tool proposed for airborne operation. First the paper summarises some basic gravity theory followed by a brief resume of the theory of 2-D Fourier transformations. The errors present in any measurement of gravity gradient are then discussed which include alignment and scale factor errors inherent in any in-line gravity gradiometer and tilt and centrifugal acceleration errors. Sections, 6-12 then discuss the Exploration Superconducting Gravity Gradiometer tool (SGG) proposed for airborne surveys - its basic principles, its alignment circuitry, its intrinsic noise, its mathematical analysis and its basic design.

## 2.Theory – Gravity and Gravity Gradiometry

The gravity field from an extended body is most easily understood in terms of its gravity scalar potential $\Phi(r)$ at $r$,

$$\Phi(r) = G\int \frac{\rho(r')}{|r'-r|} d^3r' \tag{1.1}$$

where $\rho(r')$ is the density of material at position $r'$ and $G = 6.668\times10^{-11} Nm^2kg^{-2}$ is the gravitational constant. Gravity and gravity gradients are easily calculated from the scalar potential and in cartesian coordinates

$$g(r) = \nabla\Phi(r) = \frac{\partial\Phi}{\partial x}\hat{i} + \frac{\partial\Phi}{\partial y}\hat{j} + \frac{\partial\Phi}{\partial z}\hat{k} \tag{1.2}$$

Gravity gradient is used to describe how a particular component of gravity varies with position, e.g.

$$\begin{aligned} g_x(r+\delta r) &= g_x(r) + \frac{\partial^2\Phi}{\partial x^2}\delta x + \frac{\partial^2\Phi}{\partial y\,\partial x}\delta y + \frac{\partial^2\Phi}{\partial z\,\partial x}\delta z \\ &= g_x(r) + \Gamma_{xx}\delta x + \Gamma_{xy}\delta y + \Gamma_{xz}\delta z \end{aligned} \tag{1.3}$$

The gravity gradient tensor, $\Gamma$, is as follows

© ARKeX 2010

$$\Gamma = \begin{vmatrix} \Gamma_{xx} & \Gamma_{xy} & \Gamma_{xz} \\ \Gamma_{yx} & \Gamma_{yy} & \Gamma_{yz} \\ \Gamma_{zx} & \Gamma_{zy} & \Gamma_{zz} \end{vmatrix} = \begin{vmatrix} \frac{\partial^2\Phi}{\partial x^2} & \frac{\partial^2\Phi}{\partial y\partial x} & \frac{\partial^2\Phi}{\partial z\partial x} \\ \frac{\partial^2\Phi}{\partial x\partial y} & \frac{\partial^2\Phi}{\partial y^2} & \frac{\partial^2\Phi}{\partial z\partial y} \\ \frac{\partial^2\Phi}{\partial x\partial z} & \frac{\partial^2\Phi}{\partial y\partial z} & \frac{\partial^2\Phi}{\partial z^2} \end{vmatrix} \tag{1.4}$$

It is a symmetric tensor, since the order of differentiation of a scalar quantity is irrelevant and, because gravity is a central force obeying Laplace's equation in free space, the sum of the diagonal components is zero for an inertial frame of reference. Thus there are only five independent components of the gravity gradient tensor.

For a spherical body of mass $M$ whose density is a function of radius only, along the radial direction, in spherical polars,

$$\Phi(r) = \frac{GM}{r},\ g_r = -\frac{GM}{r^2},\ \Gamma_{rr} = \frac{2GM}{r^3} \tag{1.5}$$

where $r$ refers to distance from centre of object. Other components can easily be calculated and other co-ordinate systems can be used, the main point to note here is that gravity gradient has a more rapid variation with position than does gravity so it falls away quicker from its maximum value near a mass anomaly. This ultimately translates to gravity gradient providing better estimation of edge location than does gravity.

## 3. **Theory – Fourier Transforms and Gravity Surveys**

The gravitational scalar potential is the primary quantity and, once determined, all gravitational quantities follow. Below it is shown how, using 2-D Fourier transformations, it is possible to deduce the scalar potential at all positions outside the surface of the earth by measuring any derivative of the scalar potential over a large surface above the earth. Once this is done, all quantities can be forward calculated and this removes the difficulty of not being able to transform gravity gradients between frames of reference if all components are not known. In the following, all quantities are deduced/measured over an $x-y$ plane at height $z_0$.

The 2-D Fourier transform of the scalar potential $\Phi(x,y,z_0)$ is

$$\Im_{k_x,k_y}(\Phi) = \int_{-\infty}^{\infty}\int_{-\infty}^{\infty}\Phi(x,y,z_0)e^{-ik_x x}e^{-ik_y y}dxdy \tag{2.1}$$

The inverse transform of (2.1) recovers the scalar potential

$$\Phi(x,y,z_0) = \int_{-\infty}^{\infty}\int_{-\infty}^{\infty}\Im_{k_x,k_y}(\Phi)e^{ik_x x}e^{ik_y y}dk_x dk_y \tag{2.2}$$

Thus, once the Fourier transform of the scalar potential is known over this plane, the scalar potential can be deduced.

Next consider the Fourier transformation of $g_x = \frac{\partial\Phi}{\partial x}$

$$\Im_{k_x,k_y}\left(\frac{\partial\Phi}{\partial x}\right) = \int_{-\infty}^{\infty}\int_{-\infty}^{\infty}\frac{\partial\Phi(x,y,z_0)}{\partial x}e^{-ik_x x}e^{-ik_y y}dxdy \tag{2.3}$$

Fourier transform manipulations or integration by parts yields

$$\Im_{k_x,k_y}\left(\frac{\partial\Phi}{\partial x}\right) = ik_x\int_{-\infty}^{\infty}\int_{-\infty}^{\infty}\Phi(x,y,z_0)e^{-ik_x x}e^{-ik_y y}dxdy \tag{2.4}$$

Inspection of (2.4) and (2.1) reveals

$$\Im_{k_x,k_y}\left(\frac{\partial\Phi}{\partial x}\right) = ik_x\Im_{k_x,k_y}(\Phi) \tag{2.5}$$

Thus a particular component of the Fourier transform of the gravity field is simply related to the same component of the Fourier transform of the scalar potential. Once this is known, it is then straightforward to invert this transformation to recover the scalar potential as follows.

$$\begin{aligned}\Phi(x,y,z_0) &= \Im_{x,y}^{-1}\left[\frac{1}{ik_x}\Im_{k_x,k_y}\left(\frac{\partial\Phi}{\partial x}\right)\right] \\ &= \int_{-\infty}^{\infty}\int_{-\infty}^{\infty}\frac{1}{ik_x}\Im_{k_x,k_y}\left(\frac{\partial\Phi}{\partial x}\right)e^{ik_x x}e^{ik_y y}dk_x dk_y\end{aligned} \tag{2.6}$$

The interpretation of (2.6) is that it is possible to deduce the scalar potential over a particular surface by from a measurement of one of the horizontal components of gravity over the surface.

Next consider $\Gamma_{xy} = \frac{\partial}{\partial y}\frac{\partial\Phi}{\partial x}$ whose Fourier transform is

$$\Im_{k_x,k_y}\left(\frac{\partial^2\Phi}{\partial y\partial x}\right) = \int_{-\infty}^{\infty}\int_{-\infty}^{\infty}\frac{\partial^2\Phi(x,y,z_0)}{\partial y\partial x}e^{-ik_x x}e^{-ik_y y}dxdy \tag{2.7}$$

As above, manipulation yields

$$\begin{aligned}\Im_{k_x,k_y}\left(\frac{\partial^2\Phi}{\partial y\partial x}\right) &= (i)^2 k_x k_y\int_{-\infty}^{\infty}\int_{-\infty}^{\infty}\Phi(x,y,z_0)e^{-ik_x x}e^{-ik_y y}dxdy \\ &= -k_x k_y\Im_{k_x,k_y}(\Phi)\end{aligned} \tag{2.8}$$

The scalar potential can be derived by inversion as before

$$\begin{aligned}\Phi(x,y,z_0) &= \Im_{x,y}^{-1}\left[-\frac{1}{k_x k_y}\Im_{k_x,k_y}\left(\frac{\partial}{\partial y}\frac{\partial\Phi}{\partial x}\right)\right] \\ &= \int_{-\infty}^{\infty}\int_{-\infty}^{\infty}\frac{-1}{k_x k_y}\Im_{k_x,k_y}\left(\frac{\partial}{\partial y}\frac{\partial\Phi}{\partial x}\right)e^{ik_x x}e^{ik_y y}dk_x dk_y\end{aligned} \tag{2.9}$$

These deceptively simple relations, (2.6) and (2.9), indicate that, if any of $g_x, g_y, \Gamma_{xx}, \Gamma_{xy}, \Gamma_{yy}$ is measured over a plane, the scalar potential can be deduced over that plane and hence all its derivatives wrt $x,y$ can be forward calculated.

The treatment can be continued for any $x,y$ derivative of the scalar potential and in general, (2.5) and (2.8) become

$$\Im_{k_x,k_y}\left(\frac{\partial^n}{\partial y^n}\frac{\partial^m \Phi}{\partial x^m}\right)=\left(ik_x\right)^m\left(ik_y\right)^n\Im_{k_x,k_y}\left(\Phi\right) \qquad (2.10)$$

Thus, any of the $x,y$ derivatives on the survey plane can be used to calculate $\Phi\left(x,y,z_0\right)$. Of course, once the scalar potential is known over the $z_0$ plane, any of its spatial derivatives can be forward calculated directly.

In order to use any of the $z$ derivatives of the scalar potential, further analysis is needed. In the case of gravity gradients, the Fourier transform of Laplace's equation requires

$$\Im\left(\Gamma_{xx}\right)+\Im\left(\Gamma_{yy}\right)+\Im\left(\Gamma_{zz}\right)=0 \qquad (2.11)$$

which, following similar treatment to that above yields

$$\begin{aligned}\Phi\left(x,y,z_0\right)&=\Im_{x,y}^{-1}\left[\frac{1}{k_x^{\,2}+k_y^{\,2}}\Im_{k_x,k_y}\left(\frac{\partial^2\Phi}{\partial z^2}\right)\right]\\&=\Im_{x,y}^{-1}\left[\frac{1}{\left|k\right|^2}\Im_{k_x,k_y}\left(\Gamma_{zz}\right)\right]\end{aligned} \qquad (2.12)$$

The other $z$ derivatives are a little more difficult to deduce and the treatment is beyond the scope of this paper[1]. However, the final result is similar to (2.10), viz.

$$\Im_{k_x,k_y}\left(\frac{\partial^1\Phi\left(x,y,z_0\right)}{\partial z^1}\right)=\left(-\left|k\right|\right)^1\Im_{k_x,k_y}\left(\Phi\left(x,y,z_0\right)\right) \qquad (2.13)$$

The completely general expression combines (2.10) & (2.13)

$$\Im_{k_x,k_y}\left(\frac{\partial^m}{\partial x^m}\frac{\partial^n}{\partial y^n}\frac{\partial^1}{\partial z^1}\Phi\right)=\left(ik_x\right)^m\left(ik_y\right)^n\left(-\left|k\right|\right)^1\Im_{k_x,k_y}\left(\Phi\right) \qquad (2.14)$$

Thus, any derivative of the scalar potential can be measured over the $z_0$ plane and its 2-D Fourier transform is simply related to the Fourier transform of the scalar potential. By inverse transformation the scalar potential can be deduced.

$$\frac{\partial^m}{\partial x^m}\frac{\partial^n}{\partial y^n}\frac{\partial^1}{\partial z^1}\Phi=\Im_{x,y}^{-1}\left[\left(ik_x\right)^m\left(ik_y\right)^n\left(-\left|k\right|\right)^1\Im_{k_x,k_y}\left(\Phi\right)\right] \qquad (2.15)$$

That is, all derivatives of the scalar potential on the $x,y,z_0$ plane can be obtained from the Fourier transformation of the scalar potential or of any of its derivatives.

With this, it is clearly possible to deduce the scalar potential at any point outside the surface of the earth (where Laplace's equation is valid) by a Taylor series expansion, and this is called upwards continuation. There is indeed a Green's identity which highlights this directly[2].

$$\Phi(\boldsymbol{r})=\frac{1}{4\pi}\int_{S_0}\left(\frac{1}{\left|r-r'\right|}\frac{\partial\Phi}{\partial n}-\Phi\frac{\partial}{\partial n}\frac{1}{\left|r-r'\right|}\right)dS' \qquad (2.16)$$

where $S'$ is the surface on which the scalar potential and its derivative with respect to the outward normal is known.

In the following sections, gravity gradiometers are described in general terms and the proposed exploration SGG is described in detail. For a fuller treatment of the issues relating to the SGG the reader is referred to Chan and Paik[3].

## 4.In-line Gravity Gradiometer, Basic Theory, Errors

The general schematic for an in-line gravity gradiometer is shown in Figure 1 where the two proof masses, $m_1, m_2$ have sensitive axes for detection $\hat{n}_1, \hat{n}_2$. The displacement of the proof mass centres of gravity is represented by $\ell, \hat{\ell}, \left|\ell\right|$ which are the vector, the unit vector and the base line of the instrument.

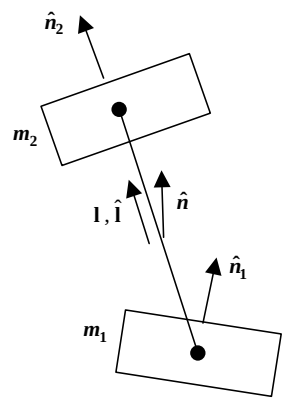


Figure 1. Schematic of in-line gravity gradiometer

In general, such a gravity gradiometer measures $\Gamma_{xx}$ as

$$\Gamma_{xx}=\frac{1}{\mathrm{l}}\left(\sigma_2 f_2.\hat{n}_2-\sigma_1 f_1.\hat{n}_1\right) \qquad (3.1)$$

where $f_1, f_2, \sigma_1, \sigma_2$ represent the specific force at and the scale factors of each accelerometer. The specific force is

$$f=g_{dc}+g(t)+a_{dc}+a(t)=f_{dc}+f(t) \qquad (3.2)$$

In order to discuss alignment and scale factor errors in the system the following notation is used.

$$\begin{aligned}&\hat{n}=\tfrac{1}{2}\left(\hat{n}_1+\hat{n}_2\right)\\&\delta\hat{n}=\hat{n}_2-\hat{n}_1\perp\hat{n},\hat{\mathrm{l}}\\&\delta\hat{\mathrm{l}}=\hat{\mathrm{l}}-\hat{n}\perp\hat{n},\hat{\mathrm{l}}\\&\delta\sigma=\sigma_2-\sigma_1\end{aligned} \qquad (3.3)$$

For the pair of accelerometers, these represent the average orientation of their sensitive axes, the non parallelism of their sensitive axes, the offset in their centres of gravity and the difference in their scale factors. In general, these will all be time dependent.

In the event that the gravity gradiometer is placed in an environment where there is zero gravity gradient, i.e. $g_1 = g_2$, the apparent gravity gradient "measured" by the instrument is

$$\delta\Gamma_{xx} = \frac{\delta\sigma(t)}{\mathrm{l}} f.\hat{n} + \frac{1}{\mathrm{l}}\delta\hat{n}.f(t) + \left(\delta\hat{\mathrm{l}} \times \hat{n}\right).\alpha(t) \qquad (3.4)$$

where $f$, $f(t)$, $\alpha(t)$ are respectively, the average total acceleration (including platform motion), the time dependent part of the total acceleration, and the angular accelerations.

Inspection of (3.4) shows that the total acceleration vector in the direction of the sense axis (static plus platform) couples into the measureed gravity gradient via scale factor errors (noise, drift and difference). Further, the linear and angular accelerations about orthogonal degrees of freedom couple in via the alignment errors. For a gravity gradiometer to work in a hostile airborne environment, these errors have to be either eliminated by design/setup or measured and removed in software, and usually a combination of both.

## 5. Centrifugal Acceleration and Tilt Errors

The above treatment did not consider the non inertial nature of the measurement frame of reference of the gravity gradiometer. For an instrument moving with an instantaneous angular rate $\Omega(t)$ and total linear acceleration $a(t)$, both with respect to an inertial frame of reference, the equation of motion for each proof mass with respect to the platform is given by[3,4]

$$\left.\frac{\partial^2 r}{\partial t^2}\right|^* = \nabla\Phi - \Omega\times\left(\Omega\times r\right) - 2\Omega\times\left.\frac{\partial r}{\partial t}\right|^* - \left.\frac{\partial\Omega}{\partial t}\right|^* \times r - a(t) \qquad (4.1)$$

where starred quantities are evaluated in the platform frame of reference. In order to obtain the desired derivative of the scalar potential, the correction terms are difficult to obtain with the desired accuracy. The best that can be obtained, including use of state of the art stabilised platform and GPS/INS systems to deduce platform accelerations, $a(t)$, is to deduce gravity to an accuracy $\approx 5mgal/Hz^{1/2}$ ($\approx 0.5mgal$ over ca. $100s$ period, i.e. ca. $5-10km$ wavelength).

Gravity gradient in the platform frame of reference is obtained by differentiating (4.1) to yield

$$\Gamma_{ij}^{\ *} = \Gamma_{ij} - \left(\Omega_i\Omega_j - \Omega^2\delta_{ij}\right) + \sum_k \varepsilon_{ijk}\alpha_k(t) - 2\Omega_i\left(\delta\Omega_j\right) \qquad (4.2)$$

where $\Gamma_{ij}$ is the true gravity gradient signal from the earth, $\alpha_k(t) = \frac{\partial\Omega_k^{\ *}}{\partial t}$ is the angular acceleration of the platform with respect to an inertial frame, $\delta\Omega_j$ is the relative angular acceleration between platform and SGG sensor and $\varepsilon_{ijk}$ is the Levi-Civita symbol which is zero if any two indices are the same, 1 if order is $xyz\ (yzx, zxy)$ or $-1$ if order is $xzy\ (zyx, yxz)$.

Equation (4.2) indicates a number of important points. First, the last term is usually very small and can be deduced from a knowledge of measured angular acceleration, this being obtained either from the stabilised platform or from the instrument itself, as discussed later in this paper. Second, the angular acceleration is usually much larger than any off diagonal gravity gradient term so $\Gamma_{ij}^{\ *}$ as measured is almost pure angular acceleration. Third, any diagonal component of gravity gradient, $\Gamma_{ii}^{\ *}$, does not explicitly contain an angular acceleration term. Finally, any single off diagonal component explicitly contains angular accelerations but these can be removed by adding $\Gamma_{ij}^{\ *}, \Gamma_{ji}^{\ *}$ to yield

$$\begin{aligned}\Gamma_{ij}(sym)^* &= \frac{1}{2}\left(\Gamma_{ij}^{\ *} + \Gamma_{ji}^{\ *}\right) \\ &= \Gamma_{ij} - \left(\Omega_i\Omega_j - \Omega^2\delta_{ij}\right) - \left(\Omega_i\delta\Omega_j + \Omega_j\delta\Omega_i\right)\end{aligned} \qquad (4.3)$$

By subtracting the two components rather than adding them, it is possible to measure the angular acceleration and remove any small corruption due to off diagonal gravity gradient

$$\begin{aligned}\Gamma_{ij}(asym)^* &= \frac{1}{2}\left(\Gamma_{ij}^{\ *} - \Gamma_{ji}^{\ *}\right) \\ &= \sum_k \varepsilon_{ijk}\alpha_k(t) - \left(\Omega_i\delta\Omega_j - \Omega_j\delta\Omega_i\right)\end{aligned} \qquad (4.4)$$

The full tensor gradiometer version of our proposed exploration tool performs such a measurement.

To correct for the terms shown in (4.3) the angular rate has to be measured, either by integration of the output of an angular acceleration superconducting circuit or by use of the GPS/INS system. In general it is also desirable to stabilise the platform since the biggest angular rate terms in (4.3) relate to the angular motions of the aircraft.

The other major angular error term is due to tilt of gradiometer from its nominally aligned axes. This gives rise to a measured gravity gradient in the "wrong" orientation. The true and measured gravity gradients are related via rotation matrices

$$\Gamma_{meas} = R\cdot\Gamma_{true}\cdot R^{-1} \qquad (4.5)$$

where $R$ is the rotation matrix from what is believed to be the true frame to the actual measurement frame of reference. Again,

the terms involved in this can be measured or estimated and used to correct the gravity gradient.

All the terms in this section will benefit from the use of a stabilised platform. Indeed, if the requirement is for the errors these terms introduce to be below system noise then this sets stringent requirements on the stabilised platform and indeed upon the aircraft's own control and stabilisation scheme.

All other major errors relate to the operation of the gravity gradiometer, how it is set up, how it works and the cryogenic environment in which it needs to work.

There has been much debate over the relative merit of measuring gravity or gravity gradient. Section 3 on Fourier analysis proves that it doesn't matter which is chosen so the issue is always about the instrument which delivers the best signal to noise for the parameter to be measured. Because of the different spatial dependences of gravity and gravity gradient, a measure of gravity gradient will always be superior to one of gravity for short wavelength features or shallow objects. In fact, (1.5) gives a convenient way of looking at this because it shows that there will be a unique distance/depth at which a spherically symmetric source can give nominated values of gravity and gravity gradient.

By choosing $1E$ as the target sensitivity for gravity gradient and $5mgal$ as the target sensitivity of the best airborne gravity tool (both per root Hz), we find that the distance/depth, $d_0$ of such a source is given simply as

$$\frac{g_z}{\Gamma_{zz}} = \frac{GM}{d_0^{\,2}} \cdot \frac{d_0^{\,3}}{2GM} = \frac{d_0}{2} \tag{4.6}$$

Simple substitution shows that the proposed SGG tool will always provide cleaner data than will a state of the art airborne gravity tool for sources with depths less than $d_0 = 100km$ .

## 6.The Superconducting Accelerometer - Principles

The principles of the superconducting accelerometer and the SGG have already been established by Chan and Paik[3] so only the most important concepts will be presented here.

The main superconducting features utilised in the SGG are the Meissner effect and flux quantisation, the latter giving the low Tc SGG its inherent phenomenal stability. The SGG requires magnetic flux in all superconducting loops to be absolutely stable and the ability to pass large currents (>10Amps) through coils, wires and joints. Failure to be able to do this renders the SGG noisy at best or inoperable at worst. This is the reason for using low temperature superconductors and wires. High temperature superconductors are just not suited for this application as none of the required technologies are mature enough. In any event, the higher temperature of operation will make the system intrinsically noisier.

Low temperatures also confer mechanical stability of all construction materials used in the SGG. At $4.2K$ the thermal expansion coefficient is reduced to ca. $10^{-9}$ of its room temperature value. Cryogenic environments are also extremely stable with $50\mu K / Hz^{1/2}$ being easily achieved. Analysis readily shows that thermal noise generates changes in the length of the gradiometer and this looks like a gravity gradient noise. However, for the low temperatures of operation and for the temperature stability proposed for the exploration SGG, this noise can be shown to be less than the intrinsic SGG noise.

The principle of the superconducting accelerometer is best described by first considering the inductance of a coil placed close to a superconductor. Meissner first demonstrated that, a superconductor expels all magnetic field up to a material dependent critical field. If current is passed through a coil outside a superconductor, a superconducting surface current is generated which, at every point inside the superconductor, produces a field equal and opposite to that produced by the external coil. This surface current interacts with the current in the coil producing a repulsive force between the coil and the superconductor. For simple geometries, it is easy to show that both the field outside the superconductor and the force between the superconductor and coil are as if there is an image coil within the superconductor. This image coil is exactly the same distance behind the superconducting surface as the real coil is in front of it and this image coil carries exactly the same current but with opposite sign. This is illustrated in Figure 2 for a flat spiral "pancake" coil.

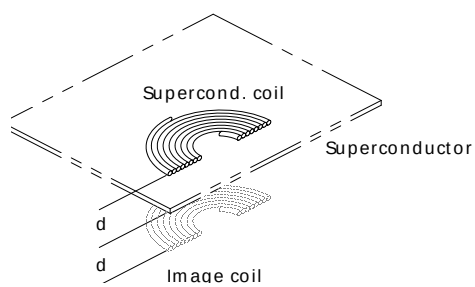


Figure 2. Superconducting "image" coil construction

It is also straightforward to calculate the inductance of this image coil which is, in fact the mutual inductance between the coil and the surface current or the coil and its image. Note first that, for a flat pancake coil in this geometry, the coil-image coil model proves that the magnetic field is confined to the region between the coil and the superconductor (note that there is no field in superconductor). This field is simply

$$B = \mu_0 n i \tag{5.1}$$

where $n =$ turns/m and $i$ is the current in the coil. The total energy in this system is simply the field energy per unit volume times the volume between coil and seuperconductor.

$$E = \frac{B^2}{2\mu_0} Ax = \frac{1}{2}\mu_0 n^2 Axi^2 \tag{5.2}$$

from which it is clear that the inductance of the coil is

$$L = \mu_0 n^2 A x + O\left(x^2\right) \tag{5.3}$$

This is the first crucial result and shows that, to first order, the inductance of the pancake coil is proportional to its separation from the superconductor. If the coil moves relative to the superconductor, its inductance will change. The first non linear term is easily understood since the field will start falling off from its maximum value at a distance ： $x$ from the edges of the coil. Thus the effective coil area is reduced from its purely geometric value by an area proportional to the perimeter of the coil multiplied by its separation from the superconductor.

Above it was demonstrated that there is a repulsive force on a "proof mass" when a current is passed through a coil in its vicinity and this force is always present when the current flows. This force follows from the energy (5.3)

$$F = \frac{1}{2}\frac{\partial L}{\partial x} i^2 = \frac{1}{2}\mu_0 n^2 A i^2 + O(x) \tag{5.4}$$

The stiffness of this magnetic spring is determined by coil non linearities. Note also that the sign of the current is irrelevant, it is its magnitude which determines the force.

The next step in understanding the SGG is to consider what happens when the pancake coil-proof mass system is placed within a closed superconducting loop as illustrated in Figure 3.

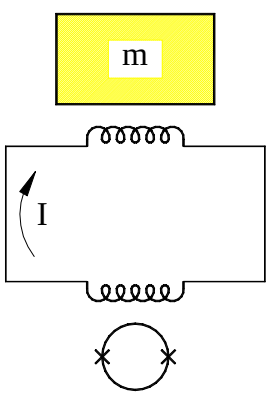


Figure 3 Superconducting accelerometer schematic

It is a truly remarkable property of superconductors that the magnetic flux in a superconducting loop, once set, is impossible to change. The flux "set" in the loop is that flux which was in the loop as the superconductor passed through its transition temperature. The "set" flux is absolutely stable and has no noise on it. This is the crucial issue for operation of the superconducting accelerometer. In reality this flux is quantised but the unit, $\Phi_0 = 2.07 \times 10^{-15} Wb$ , is so small that in practical terms it doesn't affect operation of the SGG – in operation, the SGG there contain ； $10^{11}\Phi_0$ in many loops.

Whenever the proof mass moves, in response to an acceleration or change in gravity, the coil inductance changes and the circulating current must change to preserve the original flux in the loop. This new current exerts a different force, given by (5.4) and the system stiffness is now dominated by this effect. The change in current is detected by a SQUID, a highly sensitive superconducting magnetic flux detector with resolution $\approx 3 \times 10^{-6} \Phi_0 / Hz^{1/2}$ . The SQUID is a null detector and will only respond to changes in flux which are transformer coupled from the loop.

This is the superconducting accelerometer. From the simple description given above, it is immediately obvious how important it is that flux quantisation works and that the SQUID is a null detector of unparallelled sensitivity. When the flux transfer calculation is done properly, it transpires that the noise level of the SGG effectively detects flux/current changes of ： $10^{-13}$ of their dc values.

## 7. The Superconducting Gravity Gradiometer

The schematic for a superconducting gravity gradiometer is shown in Figure 4 below where the SGG is assumed to be sensitive to gravity changes in the vertical direction. To understand the operation of the SGG requires understanding of the principles of the superconducting accelerometer with additional ingredients determined by fact that there are two masses and two loops.

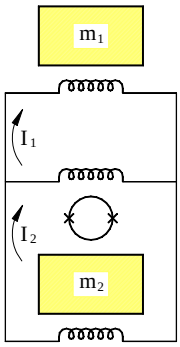


Figure 4 Schematic of Superconducting Gravity Gradiometer

First consider that the SGG is subjected to a common gravity or acceleration such that both proof masses move the same distance in the same direction, assumed downwards. This causes the inductances of both pancake coils to decrease. Flux quantisation for each superconducting loop therefore requires both $I_1, I_2$ to increase. Since these two currents flow in opposite directions through the inductor coupling to the SQUID, the changes tend to cancel one another. The system is "balanced" when the changes cancel one another completely. The SQUID does not then see a common mode gravity signal.

Note that the current through the outer loop is the average of $I_1, I_2$ so, with both currents increasing, there is a measurable current change around this loop. This current can be measured by coupling to another SQUID loop using the additonal transformer as indicated in Figure 5 below.

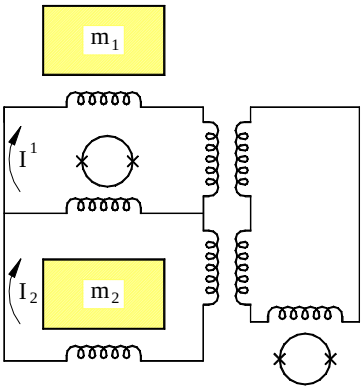


Figure 5. SGG with additional coupling inductor for outer loop

Next consider what happens if there is a differential gravity applied to the SGG with the top proof mass moving upwards and the bottom proof mass moving down. This causes $I_1$ to decrease and $I_2$ to increase. There is therefore a net current flowing through the central arm of the SGG. When the SGG is balanced, the two current changes are equal in magnitude. This circuit therefore detects gravity gradient through its central arm. In the outer loop these current changes flow in different directions so there is no change in the average of $I_1, I_2$ so such changes would not couple to a SQUID detecting common mode motion as in Figure 5.

All circuits in the SGG are generically identical to those presented in Figure 4 and Figure 5 and have the same general properties related to flux quantisation and balance. The other property they have relates to current flow through central and outer arms of the SGG. These are always related to orthogonal degrees of freedom, either differential mode and common mode, as described here, angular acceleration and transverse linear acceleration and so on.

It has been shown above, that the stability conferred on all SGG circuits by flux quantisation means that the scale factors between applied acceleration and current output remains absolutely constant. Because the gravity gradient function is performed within such circuits in this "current-differencing" SGG, the balance remains stable absolutely stable and the DM output is a true measure of the gravity gradient.

Of course, it is essential that mechanical stability of components through temperature fluctuations does not cause apparent gravity gradients. Fortunately this is an extremely small effect at low temperatures and, by choosing the right materials and a quiet cryogenic environment, the errors produced by this process will be smaller than the intrinsic noise of the SGG.

## 8. An SGG exploration tool

The basic concepts of an SGG have been elaborated above. The general circuit used in the exploration tool proposed is of the type shown in Figure 6, which is the differential mode detection circuit. Here coils interact with opposite faces of the proof masses and in most circuits the currents in the outer loops are coupled to additional SQUIDs as shown in Figure 5.

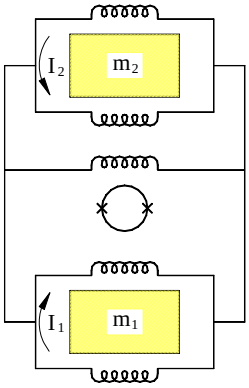


Figure 6 Differential mode circuit for exploration SGG

In general, the explanation of the workings of these circuits is similar is all cases. All that is needed is knowledge of the coil parameters and on what proof mass faces the coils interact. In this system there are no mechanical springs interacting with the proof mass, only magnetic ones. The proof masses are levitated against gravity by passing large currents through the necessary coils and the magnetic springs are formed by the use of closed superconducting loops with large circulating currents. Large currents are needed because, for operation in the airborne environment, it is necessary to stiffen the SGG as much as possible against all accelerations applied through the platform. Other coils interact with virtually all surfaces of the proof masses and these coils are integrated into circuits to perform the required functions.

The exploration SGG tool proposed here is designed to utilise the differential mode circuit to measure the gravity gradient signal but additionally to measure all linear and angular accelerations. These are needed, as seen in the simple error analysis above, because all major motion induced errors are related to these accelerations including the angular terms which can be obtained by integration of the angular acceleration outputs of the instrument. In general, even with the alignment technique discussed next, there will be residual errors which cannot be balanced out in hardware so it is necessary to measure the motions and use software analysis to correct the data to the final required precision.

## 9. Alignment circuit for the SGG

It was noted earlier that a perfectly aligned gradiometer will not couple to linear or angular accelerations in orthogonal degrees of freedom. In order to achieve this, the proposed tool includes patented alignment circuits to align the sensitive axes of the proof masses as illustrated in Figure 7. Without loss of generality, consider the $x, y, z$ orientations as being out of the page, to the right in the plane of the page and up. The origin is at the centre of gravity of the SGG.

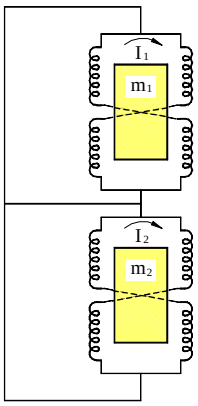


Figure 7 Alignment circuit for exploration SGG

The alignment circuit of Figure 7 is used to rotate each proof mass about its centre of gravity. First, biasing currents, $I_1 \cong I_2$ are "set" in the loops around each proof mass. These biasing currents thus flow "down" past top right and bottom left sides of each proof mass and "up" past the bottom right and top left of each proof mass.

The proof masses and coils are drawn in the approximate geometric position which they will occupy. That is, for each proof mass the coils act in pairs, one pair acting on top right and bottom left of the proof mass and the other pair acting on the top left and bottom right. If the currents are unequal through the two pairs, there will be a net torque on the proof mass and it will rotate about a line though its centre of gravity parallel to the $x$ axis.

Consider the result of a clockwise current injected into the outer loop. At the junction indicated at the top of proof mass 1, this current will divide, approximately equally. One half will add to the current going "down" past top right and bottom left of proof mass 1 and the other half will subtract from the current coming "up" past the bottom right and top left of proof mass 1. Proof mass 1 will thereby experience a net torque which will cause it to rotate counter-clockwise. This clockwise outer loop current will clearly have the same effect for proof mass 2.

That is, a current through the outer loop of this circuit causes each proof mass to rotate about its own centre of gravity about a line parallel with the $x$ axis and with the same sense. So, if the proof mass axes are offset but parallel, a current through the outer loop will bring them into colinearity with respect to the $x-z$ plane.

A current injected into the central arm of the circuit divides equally and returns through the arms of the outer loop. An argument similar to that given above shows that such a current causes each proof mass to rotate about its centre of gravity, as before, but this time they rotate in opposite senses. Thus, if the proof masses are non parallel, then a current set through the inner loop returning via the two arms of the outer loop will cause the proof mass axes to become parallel.

Thus by setting the currents in the alignment circuit of Figure 7 as described, the proof mass sensitive axes can be made colinear in the $x-z$ plane.

A similar circuit to that of Figure 7 allows the two sense axes to be brought into colinearity in the $y-z$ plane.

This scheme, therefore, has the ability to actively align the two proof mass sense axes and make them completely colinear.

This alignment scheme is based around the same generic superconducting circuitry used for the detection circuits so has the same flux quantisation benefits. The alignment errors are stable for this instrument and the above description indicates how they can be minimised. It is anticipated that this scheme will allow "hardware" set rejection for linear accelerations to be improved from a mechanical assembly alignment $\square 10^{-3}$ to $\square 10^{-7}$ leaving software to reject another two to three orders of magnitude to achieve the required rejection. For angular accelerations, the total rejection required is a couple of orders of magnitude less.

Initial results from such a scheme are shown in Figure 8 which shows the variation of the proof mass alignment with the current stored in one of the alignment circuits. It can clearly be seen that the alignment scheme works.

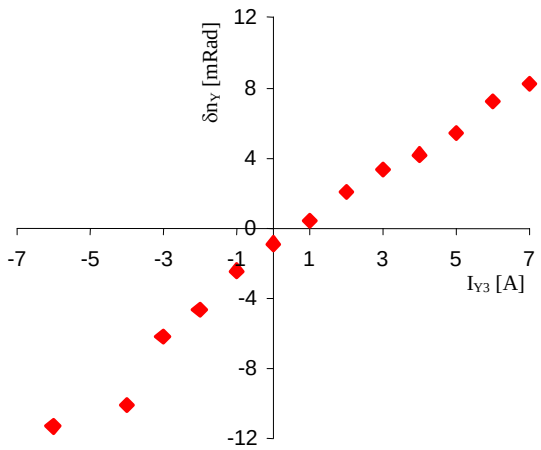


Figure 8 Alignment result for prototype gradiometer (ESA). A known horizontal acceleration is applied to the instrument and the error signal is measured. The misalignment, $\delta n_y$ is deduced from (4.4). In the above case, the proof masses become aligned with an alignment current near to 1.0 A.

## 10. Mathematics of the SGG

The theory of the SGG is relatively straightforward in principle but becomes extremely complicated when carried through to second and third order terms in the equations. The ultimate goal of the mathematics is to show that it is indeed possible to set the instrument up so that, irrespective of the accelerations to which it might be subjected, these accelerations do not couple into the differential mode. A simple linear theory has been developed by Chan and Paik[3]. Here the basic mathematical procedure is

described indicating how all non linear terms can be handled. It is straightforward to show that the SGG can always be perfectly balanced to first order but it is the second and third order terms which give rise to problems.

There are two fundamental equations to consider to deduce the dynamic behaviour of the proof masses, the flux equations and the force equations.

Flux conservation requires that, once a magnetic flux is set in a superconducting loop, it cannot change no matter where or how the proof mass moves. Thus as long as the inductance of each coil is known as a function of position and orientation then the currents in all the loops can be calculated with certainty. This current will, in general, be a non linear function of position and orientation. Assembly, orientation and manufacturing errors are straightforward to include but the complexity of the detail rapidly becomes difficult to handle.

Once the current as a function of proof mass position and orientation is known, the dynamic force equations can be used to calculate how the proof mass(es) respond to forces, gravity gradients and angular accelerations. For the analytical solution, these calculations are much better handled in the frequency domain The result of this is that the steady state solutions for the motion of the proof masses is known, including all the non linear terms.

Once the acceleration to position is determined, as above, by the force equations, this is used in the flux conservation equations to calculate the steady state currents as a function of frequency of applied acceleration.

For the gradiometer, the procedure is as follows. First, a set of currents in all the loops is chosen which correspond self consistently to a starting position/orientation for the proof masses. The gradiometer response to an applied acceleration is then calculated for all SGG circuits. The set up is changed slightly and the response to external accelerations is calculated again. The aim is to look for a starting set up which achieves perfect balance over the range of external accelerations which the instrument will encounter in flight. Each circuit in the SGG is needed to calculate the response of the SGG to a given external acceleration but the currents in each circuit are determined only by the position/orientation of the proof masses and the initial currents in that circuit.

The mathematical procedure is illustrated for the single sided accelerometer in Figure 6. The flux conservation equation is,

$$\left(L_p + L_{SQ}\right)\cdot i_{circ} = \Phi_1 \tag{9.1}$$

The following notation shall be used

$$\begin{aligned} x(t) &= x(0) + x, \\ i_{circ}(t) &= i(0) + i \\ L_p(x(t)) &= L_p(x) = L(x_0) + \Lambda x + bx^2 + \ldots \\ &= L_p(x_0) + \Delta L_p(x) \end{aligned} \tag{9.2}$$

Substitution of (9.2) into (9.1) yields

$$i = -i(0)\frac{\Delta L(x)}{L_{SQ} + L(x)} \tag{9.3}$$

Note that this equation is analytically correct, it is not an approximation and this is because the inductance used in the denominator is that at the displaced position, not the inductance at the starting position. This simple modification of standard treatment allows the full analytical solution to be calculated to arbitrary order. This same technique is valid for all loops in the SGG. Note also that (5.3) and (9.3) indicate that $i$ is a polynomial function of position due to terms both in the numerator and the denominator.

Next consider the force equation which can be written as

$$m\ddot{x} = -mg\left(x(t)\right)\cdot\hat{n} - \gamma\dot{x}(t) + F_R\left(x(t)\right) + \frac{1}{2}\frac{\partial L_p}{\partial x}\left(i_{circ}(t)\right)^2 \tag{9.4}$$

where $g.\hat{n}, F_R, \gamma$ is the gravity resolved along sensitive axis at the proof mass position, other forces on the proof mass (from other circuits), and a conventional damping term. The equilibrium position is assumed to be at $x(0)$ where (9.4) becomes a self consistency condition for the currents and forces

$$0 = -mg\left(x(0)\right)\cos\theta + F_R\left(x(0)\right) + \frac{1}{2}\frac{\partial L_p\left(x(0)\right)}{\partial x}i^2(0) \tag{9.5}$$

where $g\left(x(0)\right)$ is assumed to be the gravity at time zero when the proof mass is at position $x(0)$. With nomenclature

$$\begin{aligned} &g(t).\hat{n} = g\left(x(0)\right)\cos\theta + \delta g(t) \\ &\frac{\partial L_p}{\partial x}\left(x(0) + x\right) = \frac{\partial \bar{L}_p}{\partial x} \\ &\frac{\partial \bar{L}_p}{\partial x} - \frac{\partial L_p}{\partial x}\left(x(0)\right) = \Delta\left(\frac{\partial L_p}{\partial x}\right) \end{aligned} \tag{9.6}$$

the dynamic equations become

$$\begin{aligned} m\ddot{x} = &-m\delta g(t) - \gamma\dot{x} + \left(F_R\left(x(0) + x\right) - F_R\left(x(0)\right)\right) \\ &+ \Delta\left(\frac{\partial L_p}{\partial x}\right)i(0)^2 + \frac{\partial \bar{L}_p}{\partial x}\left(2i(0)\cdot i + i^2\right) \end{aligned} \tag{9.7}$$

From inspection of (9.2) and (9.3) it is clear that the last two terms in (9.7) are polynomial functions of $x$. The force from the other circuits is clearly of the same form as these last two terms of (9.7) so it will also be a polynomial function of $x$. Without evaluating the terms explicitly, (9.7) will therefore be of the form,

$$m\ddot{x} = -m\delta g(t) - \gamma\dot{x} - A_1 x + A_2 x^2 + A_3 x^3 \tag{9.8}$$

The first term in this expansion is

$$A_1 = -\left.\frac{\partial F_R}{\partial x}\right|_{x(0)} + i(0)^2\left(-\frac{1}{2}\frac{\partial^2 L_p}{\partial x_1^{\,2}} + \frac{\Lambda^2}{L_{SQ} + L_p\left(x(0)\right)}\right) \quad (9.9)$$

This clearly is the "Hook's Law" stiffness of the magnetic spring. The treatment to this point has been completely general without having to choose a form for $\delta g(t)$. Exactly the same type of analysis is followed for all of the more complex SGG circuits and the route from this point on is the same as well. Progress is made by assuming a particular frequency for the applied acceleration – the analytical treatment cannot be continued in the time domain. Assuming

$$\delta g(t) = g(\omega)e^{jwt} \quad (9.10)$$

it is sensible to look for a steady state solution of the form

$$x = x_1(\omega)e^{jwt} + x_2(\omega)e^{2jwt} + x_3(\omega)e^{3jwt} + \ldots \quad (9.11)$$

where the expressions for the coefficients of the frequency components will be expressed in terms of $A_1, A_2, A_3$. The first two terms are

$$x_1(\omega) = \frac{g(\omega)}{\left(\omega_0^{\,2} - \omega^2 + j\dfrac{\omega\omega_0}{Q}\right)} \quad (9.12)$$

and

$$x_2(\omega) = \frac{A_2\left(x_1(\omega)\right)^2}{\left(\omega_0^{\,2} - 4\omega^2 + j\dfrac{2\omega\omega_0}{Q}\right)} \quad (9.13)$$

where $\omega_0^{\,2} = \dfrac{A_1}{m}$ is the resonance frequency of the system and $Q = \dfrac{\omega_0 m}{\gamma}$ is the quality factor of the resonance.

It is clear that when the accuracy is taken to higher order, the lower order terms are not affected so the treatment is always accurate to the order considered – this treatment can be carried to arbitrary accuracy. Each component, $x_n(\omega)$ includes all $A_i$ components up to and including $A_n$.

The final step in the analysis is to calculate the current as a function of applied acceleration. For this, (9.11) is substituted into (9.3) to deduce the components, $i_n(\omega)$, in (10.14) below

$$i(\omega,t) = i_1(\omega)e^{j\omega t} + i_2(\omega)e^{2j\omega t} + i_3(\omega)e^{3j\omega t} + \ldots \quad (9.14)$$

The coefficients, $i_n(\omega)$ come simply from the analysis and

$$i_1(\omega) = -\frac{i(0)}{L_{SQ} + L_p}\left\{\frac{\partial L_p}{\partial x}x_1(\omega)\right\} \quad (9.15)$$

$$i_2(\omega) = -\frac{i(0)}{L_{SQ} + L_p}\left\{\begin{array}{l}\dfrac{\partial L_p}{\partial x}x_2(\omega) \\ +\left[\dfrac{1}{2}\dfrac{\partial^2 L_p}{\partial x^2} - \dfrac{1}{L_{SQ} + L_p}\left(\dfrac{\partial L_p}{\partial x}\right)^2\right]\left(x_1(\omega)\right)^2\end{array}\right\} \quad (9.16)$$

The change in current response at the frequency of this gravity or acceleration excitation, $g(\omega)$ is obtained by substituting for $x_1(\omega)$ from (9.12) into (9.15)

$$i_1(\omega) = -\frac{i(0)}{L_{SQ} + L_p}\frac{\partial L_p}{\partial x}\frac{g(\omega)}{\left(\omega_0^{\,2} - \omega^2 + j\dfrac{\omega\omega_0}{Q}\right)} \quad (9.17)$$

Inspection of (9.9) and (9.12) reveals that the first order solution is just a classic "mass on a spring" problem with the spring constants due to the accelerometer circuit being given by two terms as discussed earlier. One of these is due to the non linearity of the pancake coil inductance and contains only terms relevant to this coil. The other term is due to the closing of the loop and includes the total loop inductance, SQUID coupling plus pancake coil and the linear coefficient of the pancake coil inductance.

The current at the fundamental frequency is also resonant and all variants of these circuits have this form. The ratio between the applied acceleration, $g(\omega)$ and the induced current $i(\omega)$ is the scale factor for the accelerometer and is denoted as $H_{gi}$.

For the gradiometer circuit shown in Figure 6, exactly the same treatment can be executed but now, as there are two proof masses, there are two degrees of freedom. The time dependent accelerations applied to each proof mass can either be in phase, i.e. common acceleration or $g_c(\omega)$, or they can be out of phase, i.e. differential acceleration or $g_d(\omega)$. The current flowing around the outer loop at balance is proportional to common mode acceleration and the current flowing through the central arm is proportional to differential mode acceleration. If the current in the central arm is labelled $i_d(\omega)$ then, in the linear approximation

$$i_d(\omega) = H_{gi}^{dc}g_c(\omega) + H_{gi}^{dd}g_d(\omega) \quad (9.18)$$

Each of the $H_{ij}^{kl}$ terms will be the sum or difference of terms which look very similar to those in (9.17).

The goal of the balance procedure is to make $H_{gi}^{dc} = 0$. For a real situation with real assembly/component tolerance errors, it is easy to achieve a first order balance at a particular frequency merely by adjusting one of the major currents around one of the proof masses. In general, however, this does not give a balance at a different frequency so the balance procedure needs to first

balance at one frequency, then change the frequency of excitation acceleration, adjust a different current to achieve balance and continue until the instrument is balanced at both frequencies. This procedure gives a wide band balance. What we are balancing in this procedure is the scale factors of the two halves of the SGG. It is possible to "prove" the existence of a perfect first order balance, i.e. one at the frequency of the applied acceleration.

In general, this wide band balance does not simultaneously balance out the higher order non-linear terms (10.16) which will be large in an airborne environment. The SGG dynamics must therefore be linearised by the use of forced feedback. This works by controlling the proof mass displacements thus ensuring that the non-linear terms are negligible.

Once the balance has been achieved, flux quantisation ensures that it is maintained. The SGG is complex to set up, but once this is done, the balance is "set". The use of the alignment scheme is incorporated into this procedure so that the final set up of the instrument rejects common mode accelerations in sense direction (primarily by adjusting currents in the differential mode circuit) and rejects accelerations in orthogonal directions by the use of the alignment scheme.

The use of (3.4) together with typical accelerations as seen in an aircraft shows that the alignment issues and scale factor match issues must be treated together and that the instrument balance will not improve unless all errors, scale factor and alignment, are improved in rotation. An extremely high scale factor balance in hardware does not necessarily give a low noise if an alignment error is causing noise injection from another degree of freedom.

It is possible to perform a real time numerical analysis of the system but it is much more time consuming to run the software. Using this scheme, the ESA design with known typical assembly and manufacturing errors has been shown to be able to achieve a wide band balance for common mode accelerations with rejection in excess of $10^8$. Extrapolating this analysis for the parameters of the exploration SGG suggests that a wide band balance to a level greater than $10^6$ is possible for the accelerations expected.

## 11. Fundamental Noise/Resolution of the SGG

Paik and Chan[3] and Vitale[5] have both analysed the fundamental noise limit of a superconducting gravity gradiometer. There are two major sources of noise viz. the noise of the SQUID readout and the Brownian motion noise of the proof masses interacting with their magnetic springs. For each of these fundamental noise sources, the noise is represented as the gravity gradient signal which would yield the same result. The full expression of noise in terms of its power spectral density (PSD) is

$$S_\Gamma = \frac{8}{ml^2}\left(\frac{k_B T}{Q}\omega_0 + \omega_0^{\,2}\cdot\frac{E_A(f)}{2\beta\eta}\right) \qquad (10.1)$$

where $Q$ is the quality factor of the differential mode resonance which has a resonance frequency $\omega_0$, $k_B$ is Boltzmann's constant, $T$ is the temperature of the SGG, $E_A(f)$ is the coupled energy sensitivity of the SQUID (one of the standard specifications for a SQUID), $\beta$ is the ratio of the differential mode energy in the differential mode circuit divided by the total energy in the differential mode resonance and $\eta$ is a coupling factor from the pancake coil inductance to the SQUID (basically the ratio of SQUID inductance to total inductance in circuit). The units of $S_\Gamma$ are $\left(ms^{-2}/m\right)^2/Hz$.

A detailed design of the exploration SGG has been carried out and the above treatment indicates that, for an airborne instrument, absolute sensitivity, although important, is not the major concern. It is quite possible to design an SGG with resolution at the $10^{-3}E/Hz^{1/2}$ level but such an instrument would be impossible to use in a hostile airborne environment with virtually all outputs being saturated. For the exploration SGG it is necessary to stiffen all modes as much as is possible by use of large coils and large currents which generate both large forces and large stiffnesses.

With the designs chosen for this instrument, which includes the proof masses and all the coils and circuits which interact with them, all parameter values for the modelling are fully calculable. The result for the exploration SGG is as shown in Figure 9 below. Note that the instrument will really only be useful at low frequencies because of the speed of the plane and its distance above the ground. This means that typical "best" spatial resolutions will be of the order of one to a few hundred metres (~flying height) which will take several seconds to fly.

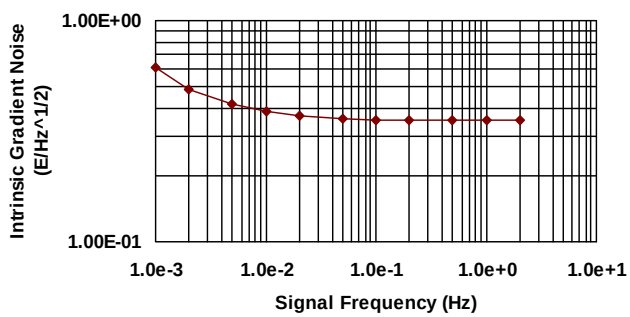


Figure 9 Fundamental resolution of exploration SGG

## 12. Design of the Exploration SGG

The design of the exploration SGG utilises similar designs to those used for the European Space Agency prototype tool developed under ESA contract 10393/93/NL/PB. The circuits are similar in design and in principle to those used to describe the basic concepts above and the SGG utilises proof masses which are as indicated in Figure 10 below. These proof masses are made from pure Niobium, weigh $100gm$ and are $50mm$ in both length and diameter. The sensitive axis for gravity gradient measurement is axial and the sense coils for both gravity gradient and axial common mode motion sense interact with the flange perpendicular to this axis inside the proof mass. Coils

acting on all the other surfaces, inside and out, are used for the alignment function and to sense all other motions when utilised in circuits as above.

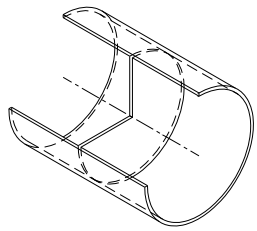

Figure 10 Exploration SGG proof mass

There are two versions of the exploration tool, the first of which will measure $\Gamma_{zz}$ and which will be made, flown and tested first, and the other a full tensor gradiometer. The $\Gamma_{zz}$ tool shall measure

| | |
|---|---|
| $a_x, a_y, a_z,$ | i.e. all linear accelerations |
| $\alpha_x, \alpha_y$ | i.e. all measurable angular accelerations |
| $\Gamma_{zz}$ | the vertical diagonal gravity gradient |

From these measurements and the use of a sophisticated GPS/INS system, all quantities needed to correct the data for all platform motions will be acquired or calculated. Analysis demonstrates that the $\Gamma_{zz}$ component is less susceptible to platform motion and better performance is therefore obtainable than for $\Gamma_{xx}$ and $\Gamma_{yy}$ for the same level of rejection of common accelerations for all directions of flying.

The mechanical layout of the exploration SGG is shown in Figure 11. This design can take six accelerometer modules to perform the full tensor gradiometer function but just two will be used in the first instrument, the $\Gamma_{zz}$ SGG.

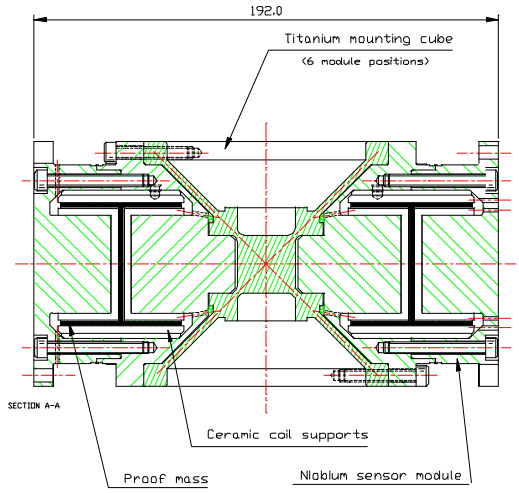


Figure 11 Cross section construction drawing of one SGG axis

Finally, it is necessary to make some comment about a stabilised platform. It is clearly desirable to remove as much noise as possible from the aeroplane. However, because of the physical amplitude of the linear motions, it is impractical to consider anything other than angular stabilisation together with passive or active isolation of low amplitude high frequency linear accelerations. Whatever is left in the way of angular and linear accelerations must be handled by the SGG itself.

Analysis shows that, if the following angular stability could be achieved, then with the exception of the centrifugal error, which cannot be rejected, angular motions will not cause errors in excess of the fundamental noise limit presented above.

$$\begin{array}{ll} 10^{-2}\,rad & \text{- Absolute pointing} \\ 10^{-4}\,rad/\sqrt{Hz} & \text{- Pointing stability} \\ 1.3\times10^{-6}\,rad/s/\sqrt{Hz} & \text{- Angular velocity} \\ 10^{-4}\,rad/s^2/\sqrt{Hz} & \text{- Angular acceleration} \end{array} \qquad (11.1)$$

The hardest of these is the angular rate error. Of course, signals above these is not death to the SGG, all that is then required is more software correction of the induced errors or, in the case of angular acceleration motion, a better intrinsic rejection.

## 13. Conclusion

The theory for the analysis and use of a superconducting gravity gradiometer has been presented. It has been shown that this tool will achieve better results than any other gravity gradiometer available today and any airborne gravity tool. The phenomenal stability of this tool is afforded by flux quantisation and the Meissner effect, fundamental quantum mechanical properties of superconductors. The design proposed for the exploration SGG has been discussed briefly and it has been demonstrated that there are parameters which allow it to achieve $1E/Hz^{1/2}$ in difficult airborne environments.

## 14. References

[1] Bracewell, *The Fourier Transform and its appluvations*,
[2] R.J.Blakely, *Potential theory in gravity*, Cambridge University Press
[3] H. A. Chan and H. J, Paik, Phys Rev D, 35(12), 3551-3571 (1987)
[4] K.R.Symon, *Mechanics*, 2nnd ed. (Addison-Wesley, Reading, MA, 1961) p278
[5] S. Vitale, GOCE Phase A study, ESA, 1999